

## ESTABLISHING CREDIBILITY OF PARTICLE METHODS THROUGH VERIFICATION TESTING

Rebecca M Brannon<sup>†</sup>, Krishna Kamojjala<sup>\*</sup> and Alireza Sadeghirad<sup>†</sup>

<sup>† \*</sup> Department of Mechanical Engineering, University of Utah  
50 S. Central Campus Dr., Salt Lake City, UT 84108, USA  
e-mail: rebecca.brannon@utah.edu, krishna.kamojjala@gmail.com, and  
alireza.sadeghirad@utah.edu

**Key words:** Verification, ring vortex, MMS, MPM, CPDI

**Abstract.** Within the particle methods community, standard benchmark tests are needed to demonstrate that the governing equations are solved correctly. Whereas the finite element method (FEM) has long-established basic verification standards (patch tests, convergence testing, etc.), no such standards have been universally adopted within the particle method community. As with FEM, particle methods must continue to pass patch tests, convergence, and frame/basis indifference. Of greater contemporary value is the establishment of additional verification tests that exercise particle methods in massive-deformation problems involving complicated geometries, for which they purport to be superior to traditional finite-element methods. Two large-deformation verification problems, applicable to any constitutive model, are proposed to serve as standardized verification tests suitable to quantify accuracy, robustness, and convergence of particle methods. These new verification tests not only simultaneously confirm basis and frame indifference, but one of them also involves very large shear strains which are common in the application of the particle methods to penetration problems. One of these problems involves traction-free boundaries, which is the only boundary condition handled naturally in most particle methods. The other problem separately allows testing of boundary conditions.

### 1 Introduction

Verification and validation of codes with complicated numerical constitutive models is very important to establish confidence in the correctness and accuracy of these codes. Verification demonstrates that the governing equations are solved correctly in the code, whereas validation provides evidence that the equations themselves are realistic.

This paper defines two large-deformation problems, applicable to any constitutive model, that may serve as verification tests suitable to quantify accuracy, robustness, and convergence of particle methods. Both verification problems employ the method of

manufactured solutions (MMS) [1], which is an accepted standard [6, 7] for verification testing accomplished by running a simulation using the external body force field that has been analytically determined to achieve a pre-selected material motion.

The MMS approach has been extensively used in the fluid mechanics community [13], but is less frequently used in solid mechanics because of the mathematical complexity involved in deriving the analytical body force. A simple 1-D MMS for solids [8], which is constructed based on [9, 10], is already available as a familiarization exercise. Some straightforward 2-D examples may be found in [12].

The first part of this paper derives the analytical body force for the manufactured solution of a much more complicated generalized vortex deformation. Even though the displacement field for this problem is more complicated than other MMS problems in the literature, the nature of the local deformation is everywhere and at all times simple shear with superimposed rotation, thus making this problem a good candidate for general constitutive model testing since the model response must be determined analytically (or in tabular form) for only a single loading mode. This vortex problem involves traction free boundary conditions on either a circular or square domain, making the boundary conditions trivial to enforce in most particle methods. The error between the predicted material motion and the exact pre-decided motion quantifies the error of the simulation. Numerical simulation results and spatial convergence studies are presented.

A second problem, documented in detail separately [5], is similar to the generalized vortex problem in the sense that all points are subjected to identical loading modes (uniaxial strain with superimposed rotation), but includes the complication of nonzero traction on the boundary. The advantage of this MMS is that it checks the implementation of traction boundary conditions in the computational model. An even simpler preliminary test of traction boundary conditions, namely homogeneous deformation, is discussed in detail as a natural prerequisite exercise.

## 2 Generalized vortex problem

This section provides a detailed description of the MMS approach to deriving the analytical body force required to produce the pre-decided material motion (simple shear with superimposed rotation) for what we refer to as “the generalized vortex” problem. The dynamic equation of motion is:

$$\text{DIV}(\mathbf{T}) + \rho_o \mathbf{b} = \rho_o \mathbf{a} \quad (1)$$

where  $\mathbf{a}$  is the acceleration,  $\mathbf{b}$  is the body force,  $\mathbf{T}$  is the first-Piola Kirchhoff (PK1) stress,  $\rho_o$  is the initial density, and  $\text{DIV}(\mathbf{T})$  is the backwards reference divergence of  $\mathbf{T}$ , defined with respect to the Cartesian basis  $(\mathbf{E}_1, \mathbf{E}_2, \mathbf{E}_3)$  by

$$\text{DIV}(\mathbf{T}) = \frac{\partial T_{ij}}{\partial X_j} \mathbf{E}_i = \frac{\partial \mathbf{T}}{\partial \mathbf{X}} : \mathbf{I} \quad (2)$$

where “ $:$ ” is the second-order tensor inner product, and  $\mathbf{I}$  is the second-order identity tensor. The problem domain is a ring of inner radius  $a$  and outer radius  $b$ , as shown

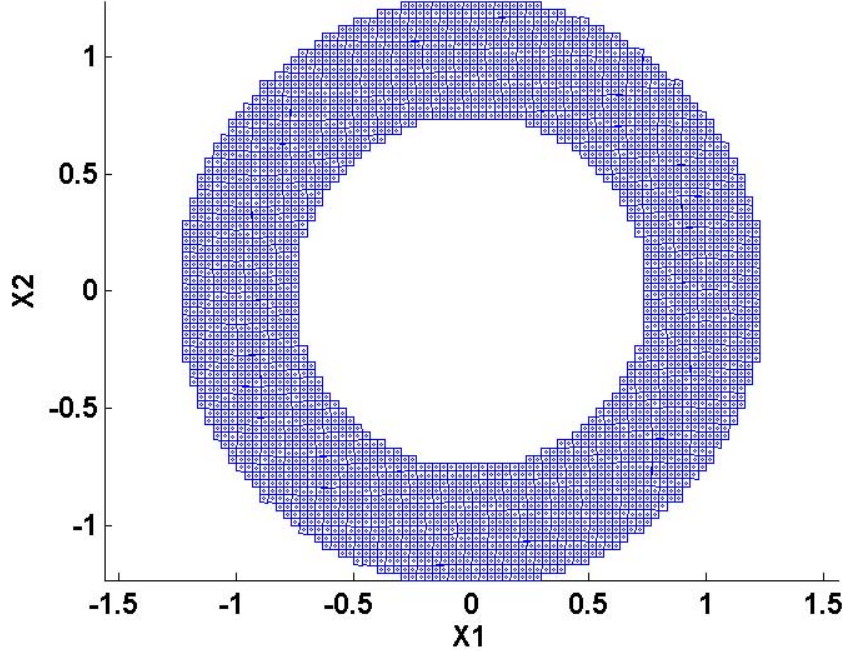


**Figure 1:** The problem domain of the generalized vortex example.

in Figure 1. The upcoming manufactured solution will have zero displacements and (to achieve traction-free boundaries) zero displacement gradients at the inner and outer radii. Thus, since material motion will occur only in the interior of the ring, this problem may be also regarded to apply on a square domain for which material outside the ring is prescribed to be stationary. This problem involves pure circular motion of all particles. The angular displacement varies with the radial coordinate, thus inducing simple shear with superimposed rotation at all times and at all spatial locations. For plane strain circular particle motion, the mapping from the initial position  $\mathbf{X}$  to the current position  $\mathbf{x}$  is given by

$$\mathbf{x} = \mathbf{Q} \cdot \mathbf{X}. \quad (3)$$

Here,  $\mathbf{Q}$  is the orthogonal tensor with components

$$\mathbf{Q} = \begin{bmatrix} \cos \alpha & -\sin \alpha & 0 \\ \sin \alpha & \cos \alpha & 0 \\ 0 & 0 & 1 \end{bmatrix} \quad (4)$$

where  $\alpha$  is the rotation angle, which varies with time and radial coordinate  $R$  but not with angular coordinate  $\Theta$ . Specifically,

$$\alpha(R, t) = g(t)h(R) \quad (5)$$

where,  $g(t)$  controls the amplitude of the deformation, and  $h(R)$  controls relative radial variation of the rotation. The  $h(R)$  function is selected in a way to ensure that material motion occurs only between the inner and outer radii,  $a$  and  $b$ . Thus,  $h(R) = 0$  for  $R < a$  and  $R > b$ . For continuous displacements, this implies that  $h(a) = h(b) = 0$ . Moreover, choosing  $h'(a) = h'(b) = 0$  ensures zero strain and hence zero traction at the boundary, which is typically easy to enforce in particle methods. The goal is to find the spatially varying body force field  $\mathbf{b}(R, \Theta)$  necessary to produce this motion.

To begin the analysis, the following lemmas are useful: for any scalar  $s$ ,

$$\frac{d\mathbf{Q}}{ds} = \frac{d\mathbf{Q}}{d\alpha} \frac{d\alpha}{ds} = \mathbf{A} \cdot \mathbf{Q} \frac{d\alpha}{ds} \quad (6)$$

where  $\mathbf{A}$  is the axial tensor associated with the rotation axis. Namely,

$$\mathbf{A} = \begin{bmatrix} 0 & -1 & 0 \\ 1 & 0 & 0 \\ 0 & 0 & 0 \end{bmatrix}. \quad (7)$$

The axial tensor has the important property that, for any vector  $\mathbf{w}$ ,

$$\mathbf{A} \cdot \mathbf{w} = \mathbf{E}_z \times \mathbf{w} \quad (8)$$

where  $\mathbf{E}_z$  is the unit cylindrical base vector along the axis of rotation. Thus, for example, noting that the position vector is  $\mathbf{X} = R\mathbf{E}_R$ ,

$$\mathbf{A} \cdot \mathbf{X} = \mathbf{E}_z \times (R\mathbf{E}_R) = R\mathbf{E}_\Theta \quad (9)$$

The following sections provide steps for determining the deformation gradient  $\mathbf{F}$ , divergence of the PK1 stress  $\text{DIV}(\mathbf{T})$ , and acceleration  $\mathbf{a}$  required to ultimately solve (1) for the body force.

## 2.1 Deformation gradient and divergence of PK1 stress

Differentiating (5), the gradient of the rotation angle is given by

$$\frac{d\alpha}{d\mathbf{X}} = g(t) \frac{dh}{dR} \frac{dR}{d\mathbf{X}} = g(t)h'(R)\mathbf{E}_R. \quad (10)$$

The deformation gradient is found by taking the derivative of (3)

$$\mathbf{F} = \frac{d\mathbf{x}}{d\mathbf{X}} = \mathbf{Q} + \mathbf{X} \cdot \frac{d\mathbf{Q}^T}{d\alpha} \frac{d\alpha}{d\mathbf{X}}. \quad (11)$$

Using (6),(10), (9), and the fact that  $\mathbf{Q}^T \cdot \mathbf{A} \cdot \mathbf{Q} = \mathbf{A}$  , we have

$$\mathbf{F} = \mathbf{Q} \cdot (\mathbf{I} + Rg(t)h'(R)\mathbf{E}_\Theta\mathbf{E}_R). \quad (12)$$

The terms in the parentheses represent a state of simple shear in the  $\Theta$  direction with the shear plane tangent to the circumference. The multiplication by  $\mathbf{Q}$  represents additional superimposed rotation into the current configuration. Let

$$2\xi(R) = Rh'(R). \quad (13)$$

Then the shear strain is given by

$$\epsilon(t, R) = g(t)\xi(R). \quad (14)$$

The deformation gradient in (12) may be written as

$$\mathbf{F} = \mathbf{Q} \cdot \mathbf{q} \cdot \mathcal{F} \cdot \mathbf{q}^T \quad (15)$$

where

$$\mathcal{F} = \mathbf{I} + 2\epsilon(t, R)\mathbf{E}_2\mathbf{E}_1 \quad \text{and} \quad \mathbf{q} = \begin{bmatrix} \cos \Theta & -\sin \Theta & 0 \\ \sin \Theta & \cos \Theta & 0 \\ 0 & 0 & 1 \end{bmatrix}. \quad (16)$$

Note that

$$\mathbf{F} = \mathbf{r} \cdot \mathcal{F} \cdot \mathbf{q}^T \quad \text{where} \quad \mathbf{r} = \begin{bmatrix} \cos \theta & -\sin \theta & 0 \\ \sin \theta & \cos \theta & 0 \\ 0 & 0 & 1 \end{bmatrix} \quad (17)$$

Here,  $\theta = \Theta + \alpha = \Theta + g(t)h(R)$ , which is the angular coordinate of the particle in the deformed configuration. Note that  $\mathcal{F}$  is an angle-independent “baseline” deformation representing simple shear without superimposed rotation. Further note that  $\frac{d\mathcal{F}}{dR} = 2g(t)\xi'(R)\mathbf{E}_2\mathbf{E}_1$ . Also,  $\mathbf{q}$  is independent of  $R$ , and  $\frac{d\mathbf{q}}{d\Theta} = \mathbf{A} \cdot \mathbf{q}$ . The tensor  $\mathbf{r}$  depends only on the deformed angular coordinate, but (since the deformed angle varies with radial coordinate), this tensor implicitly depends on both angular and radial coordinates. Thus, applying the chain rule,

$$\frac{d\mathbf{r}}{d\theta} = \mathbf{A} \cdot \mathbf{r}; \quad \left( \frac{\partial \mathbf{r}}{\partial \Theta} \right)_R = \mathbf{A} \cdot \mathbf{r}; \quad \left( \frac{\partial \mathbf{r}}{\partial R} \right)_\Theta = g(t)h'(R)\mathbf{A} \cdot \mathbf{r} \quad (18)$$

where subscripts are used to indicate what is held constant in partial derivatives. Let  $S$  denote the second-Piola Kirchhoff (PK2) stress associated with the deformation  $\mathcal{F}$ . Then, for an isotropic material, it follows that the PK2 stress  $\mathbf{S}$  associated with  $\mathbf{F}$  must be

$$\mathbf{S} = \mathbf{q} \cdot S \cdot \mathbf{q}^T \quad (19)$$

The first Piola-Kirchhoff (PK1) stress associated with deformation  $\mathbf{F}$  is then

$$\mathbf{T} = \mathbf{F} \cdot \mathbf{S} = \mathbf{Q} \cdot \mathbf{q} \cdot \boldsymbol{\tau} \cdot \mathbf{q}^T = \mathbf{r} \cdot \boldsymbol{\tau} \cdot \mathbf{q}^T \quad (20)$$

where  $\boldsymbol{\tau} = \mathcal{F} \cdot S$  is the PK1 stress associated with the baseline deformation  $\mathcal{F}$ , which depends on  $R$  indirectly through dependence of the shear strain on  $R$ , but this baseline PK1 stress is not dependent on the angular coordinate. Thus

$$\left( \frac{\partial \boldsymbol{\tau}}{\partial R} \right)_t = \frac{d\boldsymbol{\tau}}{d\epsilon} \left( \frac{\partial \epsilon}{\partial R} \right)_t = \frac{d\boldsymbol{\tau}}{d\epsilon} g(t) \xi'(R). \quad (21)$$

The reference gradient of PK1 stress is a third-order tensor given by

$$\left( \frac{\partial \mathbf{T}}{\partial \mathbf{X}} \right)_t = \left( \frac{\partial \mathbf{T}}{\partial R} \right)_{\Theta,t} \mathbf{E}_R + \frac{1}{R} \left( \frac{\partial \mathbf{T}}{\partial \Theta} \right)_{R,t} \mathbf{E}_{\Theta}. \quad (22)$$

Using (20), (18), and the chain rule, this equation becomes

$$\left( \frac{\partial \mathbf{T}}{\partial \mathbf{X}} \right)_t = (g(t)h'(R)\mathbf{A} \cdot \mathbf{T} + g(t)\xi'(R)\mathbf{r} \cdot \frac{d\boldsymbol{\tau}}{d\epsilon} \cdot \mathbf{q}^T) \mathbf{E}_R + \frac{1}{R} (\mathbf{A} \cdot \mathbf{T} + \mathbf{T} \cdot \mathbf{A}^T) \mathbf{E}_{\Theta}. \quad (23)$$

Referring to (2), recognizing that  $\mathbf{q}^T \cdot \mathbf{E}_R = \mathbf{E}_1$ , and using (8) to note that  $\mathbf{A}^T \cdot \mathbf{E}_{\Theta} = \mathbf{E}_R$ , the reference divergence of PK1 stress is given by

$$\begin{aligned} \text{DIV}(\mathbf{T}) = \rho_o(\mathbf{a} - \mathbf{b}) &= g(t)h'(R)\mathbf{A} \cdot \mathbf{T} \cdot \mathbf{E}_R + g(t)\xi'(R)\mathbf{r} \cdot \frac{d\boldsymbol{\tau}}{d\epsilon} \cdot \mathbf{E}_1 \\ &\quad + \frac{1}{R} (\mathbf{A} \cdot \mathbf{T} \cdot \mathbf{E}_{\Theta} + \mathbf{T} \cdot \mathbf{E}_R). \end{aligned} \quad (24)$$

In terms of the deformed angular coordinate  $\theta$ , the spatial cylindrical base vectors are

$$\mathbf{e}_r = \cos(\theta)\mathbf{E}_1 + \sin(\theta)\mathbf{E}_2 \quad \mathbf{e}_{\theta} = -\sin(\theta)\mathbf{E}_1 + \cos(\theta)\mathbf{E}_2. \quad (25)$$

Dotting (24) by these spatial cylindrical base vectors, the spatial cylindrical components of the divergence of PK1 stress are given by

$$\rho_o(a_r - b_r) = (\xi'(R) \frac{d\tau_{11}}{d\epsilon} - h'(R)\tau_{21})g(t) + \frac{1}{R}(\tau_{11} - \tau_{22}). \quad (26)$$

$$\rho_o(a_{\theta} - b_{\theta}) = (\xi'(R) \frac{d\tau_{21}}{d\epsilon} + h'(R)\tau_{11})g(t) + \frac{1}{R}(\tau_{12} + \tau_{21}). \quad (27)$$

The key advantage of the above result is that it is expressed in terms of Cartesian components of the PK1 stress corresponding to a baseline homogeneous pure shear, thus requiring the constitutive model to be evaluated only for that special case.

## 2.2 Velocity and acceleration

Using (3), (5) and (6), the velocity and acceleration of any given material particle are

$$\mathbf{v} = \dot{\mathbf{Q}} \cdot \mathbf{X} = g'(t)h(R)\mathbf{A} \cdot \mathbf{x} = R\omega\mathbf{e}_{\theta}, \quad (28)$$

$$\mathbf{a} = g''(t)h(R)\mathbf{A} \cdot \mathbf{x} - (g'(t)h(R))^2\mathbf{x} = R\dot{\omega}\mathbf{e}_{\theta} - R\omega^2\mathbf{e}_r. \quad (29)$$

where

$$\omega = g'(t)h(R) \quad \text{and} \quad \dot{\omega} = g''(t)h(R). \quad (30)$$

### 2.3 Body force

The body force vector is given by

$$\mathbf{b} = b_r \mathbf{e}_r + b_\theta \mathbf{e}_\theta. \quad (31)$$

Using (26), (27), (29), and (30), the spatial cylindrical components of the body force are

$$b_r = -R(g'(t)h(R))^2 - \frac{1}{\rho_o}((\xi'[R]\frac{d\tau_{11}}{d\epsilon} - h'[R]\tau_{21})g(t) + \frac{1}{R}(\tau_{11} - \tau_{22})), \quad (32)$$

$$b_\theta = -R(g''(t)h(R)) - \frac{1}{\rho_o}((\xi'[R]\frac{d\tau_{21}}{d\epsilon} + h'[R]\tau_{11})g(t) + \frac{1}{R}(\tau_{12} + \tau_{21})). \quad (33)$$

The Cartesian components are obtained by substituting (25) into (31).

### 2.4 Numerical simulation

The above solution applies to any nonlinear elastic constitutive model. The constitutive model selected to illustrate the solution is the following simple NeoHookean model:

$$\boldsymbol{\sigma} = \frac{\lambda \log[J]}{J} \mathbf{I} + \frac{\mu}{J} [\mathbf{F} \cdot \mathbf{F}^T - \mathbf{I}] \quad (34)$$

where,  $\lambda$  is the Lame modulus,  $\mu$  is the shear modulus,  $J$  is the Jacobian of the deformation gradient  $\mathbf{F}$  and  $\mathbf{I}$  is the identity tensor. The initial density is chosen to be  $\rho_o = 1000 \frac{kg}{m^3}$ , Young's modulus and Poisson's ratio are chosen to be  $10^3$ Pa and 0.3 respectively (corresponding to  $\lambda = 577$ Pa and  $\mu = 385$ Pa). The inner and outer radii are  $0.75m$  and  $1.25m$ , respectively. The final time of the simulation is  $T = 1s$ . The amplitude and distortion functions are taken to be  $g(t) = \sin(\frac{\pi t}{T})$  and  $h(R) = (1 - 32(R - 1)^2 + 256(R - 1)^4)$ . Based on these values the components of the body force are evaluated to be

$$b_r = -\pi^2 R (15 - 32R + 16R^2)^4 \cos[\pi t]^2 + \frac{R\mu \sin[\pi t]^2 (-64(R - 1) + 1024(R - 1)^3)^2}{\rho_o} \quad (35a)$$

$$b_\theta = -\frac{(64\mu(-45 + 188R - 240R^2 + 96R^3) + \rho_o \pi^2 R (15 - 32R + 16R^2)) \sin[\pi t]}{\rho_o} \quad (35b)$$

This manufactured solution was implemented in the open-source Uintah MPM framework [11]. The results using two integration options (called uGIMP [4] and CPDI [2]) are presented. As seen in Figure 2, the simulation becomes unstable for uGIMP, but remains stable for CPDI. Even though the CPDI method gives superior results in comparison to all predecessor MPM methods, its final configuration shown in 3 still shows clear evidence of mesh and/or particle distribution texture bias.

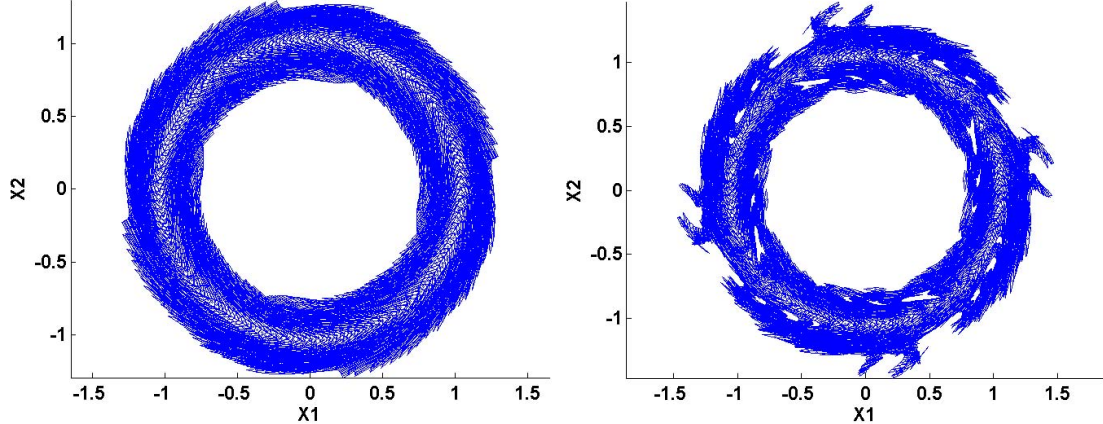


**Figure 2:** Deformed configurations for CPDI and uGIMP near the peak rotation angle

Figure 4 shows convergence properties for this example using an L<sub>2</sub> error defined by

$$L_2\text{error} = \sqrt{\frac{\sum_{N_p} \| \mathbf{u}_{\text{exact}}(x_p, t) - \mathbf{u}_{\text{app}}(x_p, t) \|^2}{N_p}} \quad (36)$$

where  $\mathbf{u}_{\text{exact}}(x_p, t)$  and  $\mathbf{u}_{\text{app}}(x_p, t)$  are the analytical and calculated displacement vectors, respectively, and  $N_p$  is total number of MPM particles. The top two plots in Figure 4 represent the time variation of error for four different mesh resolutions using CPDI and uGIMP, respectively. The bottom two plots show standard rate of convergence plots of the error as a function of cell spacing at time  $t = 1s$ . The convergence plot for CPDI shows a normal decrease in error as the resolution is increased, with a rate of convergence close to 0.8. For the uGIMP method, on the other hand, the convergence plot lacks useful information because that method was unstable or crashed by time  $t = 1s$  in all cases.

### 3 Homogeneous deformation

A 2-D homogeneous deformation MMS is illustrated here to check the implementation of traction boundary conditions in the simplest possible context. For a homogeneous deformation, the displacement field is given by

$$\mathbf{x} = \mathbf{F} \cdot \mathbf{X} \quad (37)$$

where the deformation gradient tensor  $\mathbf{F}$  varies with time, but not position. To illustrate, we consider a deformation gradient that varies linearly in time according to  $\mathbf{F} = \mathbf{I}(1 - t) + \mathcal{F}t$ , where  $\mathcal{F}$  characterizes the final deformed shape at the simulation stop time of  $t = 1s$ . As the simplest possible example, the final deformation tensor for uniaxial strain, corresponding to a stretch  $\Lambda$  in the 1-direction is

$$\mathcal{F} = \begin{bmatrix} \Lambda & 0 & 0 \\ 0 & 1 & 0 \\ 0 & 0 & 1 \end{bmatrix} \quad (38)$$

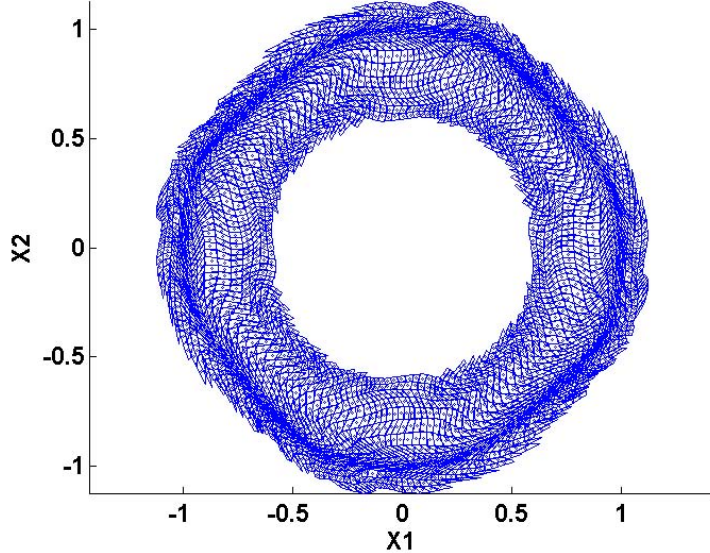


**Figure 3:** Final configuration using CPDI at  $t = 1s$

For homogeneous deformation of a homogeneous material, the gradient of stress is zero, implying, from (1), that the body force equals the acceleration. In this simple case of a linear morph of the deformation gradient from  $\mathbf{I}$  at time  $t = 0$  to  $\mathcal{F}$  at  $t = 1$ , the acceleration is zero, and hence the body force is zero. Boundary traction is given by  $\mathbf{t} = \boldsymbol{\sigma} \cdot \mathbf{n}$ , where  $\boldsymbol{\sigma}$  is the Cauchy stress and  $\mathbf{n}$  is the unit outward normal. While a linearly morphing homogeneous deformation gradient has the advantage that the required body force is zero, the initial velocity field,  $\mathbf{v} = \dot{\mathbf{F}} \cdot \mathbf{X}$ , is nonzero.

For illustration, the NeoHookean constitutive model in (34) will be applied to the uniaxial strain deformation in (38) using an initially square domain and peak stretch value of  $\Lambda = 2$ . The traction's on the four faces of the domain are

$$\mathbf{t}_1 = -\mathbf{t}_2 = \left[ \frac{\lambda \ln(\Lambda t - t + 1) + \mu((\Lambda t - t + 1)^2 - 1)}{(\Lambda t - t + 1)} \right] \mathbf{E}_1 \quad (39)$$

$$\mathbf{t}_3 = -\mathbf{t}_4 = \left[ \frac{\lambda \ln(\Lambda t - t + 1)}{(\Lambda t - t + 1)} \right] \mathbf{E}_2 \quad (40)$$

where  $\mathbf{t}_1$  is the traction on the positive x-face,  $\mathbf{t}_2$  is the traction on negative x-face,  $\mathbf{t}_3$  is the traction on positive y-face and  $\mathbf{t}_4$  is the traction on negative y-face. The initial problem domain is a unit square, discretized using  $2 \times 2$ ,  $4 \times 4$  and  $8 \times 8$  grid resolutions with two particles per cell in each direction. Young's modulus and Poisson's ratio are  $10^6 \text{Pa}$  and  $0.25$ , respectively, with the stop time of the simulation  $t = 1s$ .

Figure 5 shows the deformation at various time steps. Again adopting the error definition in (36), the displacement field errors for the three resolutions are listed in table 1. It

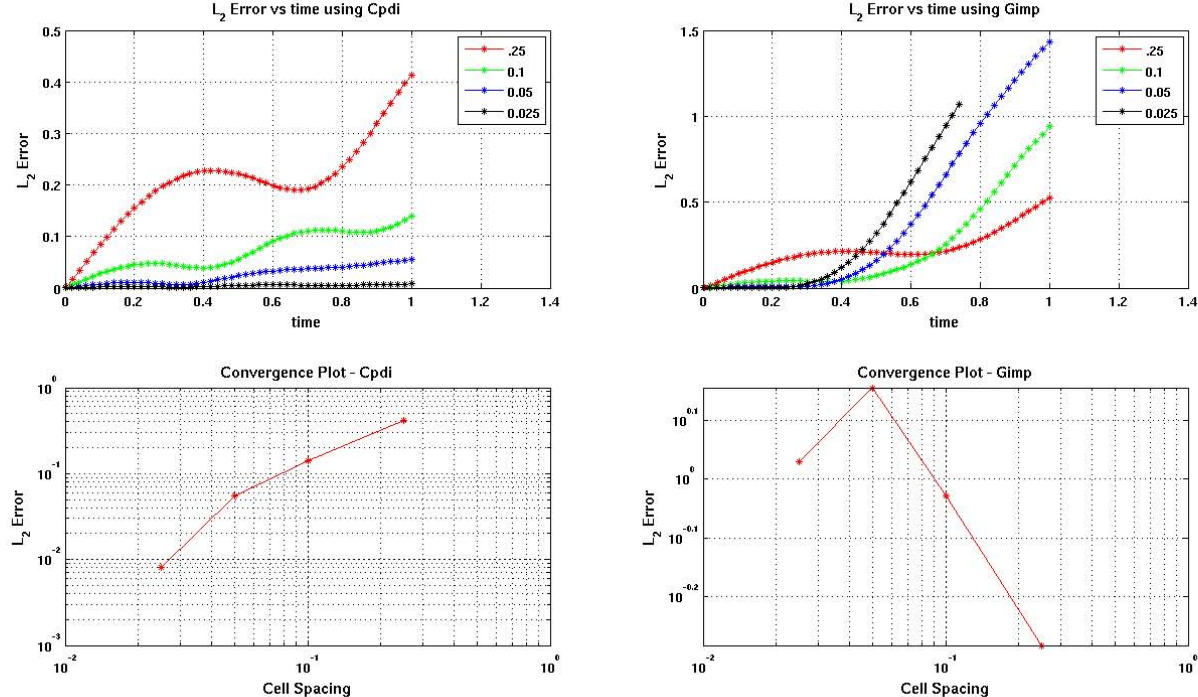


**Figure 4:** Convergence plots for the stable CPDI simulations and unstable uGIMP simulations

**Table 1:** L<sub>2</sub> error (meters) for various grid resolutions

	2×2	4×4	8×8
L <sub>2</sub> error	0.0733	0.0724	0.0724

can be seen that the problem has converged at 4×4 grid resolution. However, the failure to converge to machine precision indicates the need to investigate sources of error in the prescribed traction boundary condition algorithm for this code.

#### 4 CONCLUSIONS

- Two large-deformation verification problems, applicable to any constitutive model (but illustrated using a simple elasticity model), were presented.
- The derivation of the analytical body force for a generalized vortex problem, which involved very large shear strains with traction free boundary conditions, was presented. Numerical simulation results with spatial convergence studies were provided for this problem.
- The method of manufactured solutions (MMS) for a simple homogeneous defor-

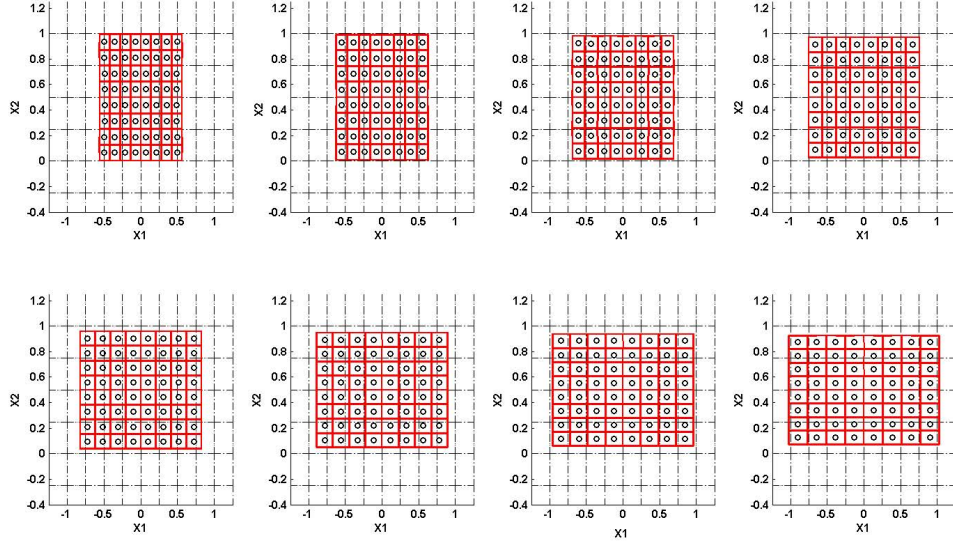


**Figure 5:** Deformed configurations of the unit square at different times

mation problem (uniaxial strain) was presented as a straightforward example of a class of problems appropriate for assessing accuracy of traction boundary conditions, which are notoriously difficult to implement in particle codes.

- These two verification problems were designed to have the same type of deformation (simple shear with superimposed rotation and uniaxial strain) at all material points. As such, these problems represent a rare case of being nontrivial MMS verification problems applicable to *any* – even highly nonlinear and history-dependent – constitutive model, provided that the response of the model to these standard loadings can be evaluated or tabulated.

## REFERENCES

- [1] Knupp, P. and Salari, K. *Verification of computer codes in Computational Science and Engineering*. Chapman and Hall/CRC, (2003).
- [2] Sadeghirad, A., Brannon, R. and Burghardt, J. “A convected particle domain interpolation technique to extend applicability of the material point method for problems involving massive deformations”, *Intl. J. Num. Meth. Engng.* (2011) accepted for publication.
- [3] Sulsky, D., Chen, E. and Schreyer, H. “A particle method for history-dependent materials”, *Comput. Meth. Appl. Mech. Eng.* (1994) **118**:179-196.
- [4] Bardenhagen, S., and Kober, E. “The generalized interpolation material point method”, *Comput. Meth. Engg. Sci.* (2004) **5**:477-495.

- [5] Kamojjala, K., and Brannon, R. "Verification of frame indifference for complicated numerical constitutive models", *ASME Early Career Technical Conference* (2011).
- [6] Schwer, L. E., et al.. "Guide to Verification and Validation in Computational Solid Mechanics", *ASME V&V* (2006).
- [7] Salari, K. and Knupp, p. *Code Verification by Method of Manufactured Solutions*. SANDIA REPORT, (2000).
- [8] Banerjee, B. "Method of Manufactured solutions". [www.eng.utah.edu/~banerjee/Notes/MMS.pdf](http://www.eng.utah.edu/~banerjee/Notes/MMS.pdf), (2000).
- [9] Batra, R.C. and Liang, X.Q. "Finite dynamic deformations of smart structures" *Computational Mechanics*.(1997)**20**:427-438.
- [10] Batra, R.C. and Love, B.M. "Multiscale analysis of adiabatic shear bands in tungsten heavy alloy particulate composites" *International Journal for Multiscale Computational Engineering*. (2006) **4(1)**:95-114.
- [11] Guilkey, J. Harman, T. et.al. *Uintah User guide*. SCI Institute Technical Report, (2009).
- [12] Wallstedt, P. and Guilkey, J. "An evaluation of explicit time integration schemes for use with the generalized interpolation material point method" *J. of Comput. Phys.*. (2008) **227**:9628-9642.
- [13] Tremblay, D., Etienne, S. and Pelletier, D. "Code verification and the method of manufactured solutions for fluid-structure interaction problems". *36th AIAA Fluid Dynamics Conference*, (2006). **2**:882-892.